

Supplementary Materials

**The use of well-defined surface organometallic complex
as a probe molecule: $[(\equiv \text{SiO})\text{Ta}^{\text{V}}\text{Cl}_2\text{Me}_2]$ shows different
isolated silanol sites on silica surface**

Yin Chen, Bin Zheng, Edy Abou-Hamad, Ali Hamieh, Bilel Hamzaoui, Kuo-wei Huang, Jean-
marie Basset*

Corresponding Authors: Jeanmarie.basset@kaust.edu.sa

King Abdullah University of Science and Technology (KAUST), KAUST Catalysis Center,
Thuwal 23955-6900, Saudi Arabia.

Support information: Table of contents

1. General procedures	3	
2. Figure S1-5: IR and NMR spectra of $(\equiv\text{SiO})\text{Ta}^{\text{V}}\text{Cl}_2\text{Me}_2$ on silica-700		5
3. Figure S6-7: NMR spectra of $(\equiv\text{SiO})\text{Ta}^{\text{V}}\text{Cl}_2\text{Me}_2/\text{Aerosil}_{(700)}\cdot\text{NEt}_3$		8
2. Figure S8-10: NMR spectra of $(\equiv\text{SiO})\text{Ta}^{\text{V}}\text{Cl}_2\text{Me}_2$ on different silica support		9
4. Figure S11-12: TEM of $(\equiv\text{SiO})\text{Ta}^{\text{V}}\text{Cl}_2\text{Me}_2$ as synthesized	11	
4. Coordinates of related structures and calculated chemical shift difference with angle		13

1. General Procedures

All experiments were carried out under inert atmosphere, using Schlenk and glove box techniques for the organometallic synthesis. For the syntheses and treatments of the surface species, experiments were carried out using high-vacuum lines (10^{-5} mbar) and glove box techniques. Toluene was purified with a SPS. Infrared spectra (transmission) were recorded on a Nicolet Magna 6700 FT spectrometer equipped with a cell under controlled atmosphere. Elemental analyses were performed at the Mikroanalytisches Labor Pascher in Germany.

Solid State Nuclear Magnetic Resonance Spectroscopy:

One dimensional ^1H MAS, ^{13}C CP-MAS and ^{29}Si CP-MAS solid state NMR spectra were recorded on a Bruker AVANCE III spectrometer operating at 400, 100 and 80 MHz resonance frequencies for ^1H , ^{13}C and ^{29}Si respectively, with a conventional double resonance 4mm CPMAS probe. The samples were introduced under argon into zirconia rotors, which were then tightly closed. The spinning frequency was set to 17, 10, and 5 KHz for ^1H , ^{13}C and ^{29}Si spectra, respectively. NMR chemical shifts are reported with respect to TMS as an external reference. For CP/MAS ^{13}C and ^{29}Si NMR, the following sequence was used: 90° pulse on the proton (pulse length 2.4 s), then a cross-polarization step with a contact time typically 2 ms, and finally acquisition of the ^{13}C and ^{29}Si signal under high power proton decoupling. The delay between the scan was set to 5 s, to allow the complete relaxation of the ^1H nuclei and the number of scans was between 3,000-5,000 for carbon, 30,000-50,000 for Silicon and 32 for proton. An apodization function (exponential) corresponding to a line broadening of 80 Hz was applied prior to Fourier transformation.

The 2D ^1H - ^{13}C heteronuclear correlation (HETCOR) solid state NMR spectroscopy experiments were conducted on a Bruker AVANCE III spectrometer using a 3.2 mm MAS probe. The experiments were performed according to the following scheme: 90° proton pulse, t_1 evolution period, cross-polarization (CP) to carbon spins, and detection of carbon magnetization under TPPM decoupling^{1,2}. For the cross-polarization step, a ramped radio frequency (RF) field centered at 75 KHz was applied to protons, while the carbon RF field was matched to obtain optimal signal. A total of 32 t_1 increments with 2000 scans each were collected. The sample spinning frequency was 8.5 kHz. A 2D Fourier transformation gives through space between pairs of neighboring carbon (in F2) and proton (in F1) nuclei. Using a short contact time (0.5 ms) for the CP step, the polarization transfer in the dipolar correlation experiment is expected to be quite selective, that is to lead to correlation only between pairs of attached ^1H - ^{13}C spins (C-H directly bonded). Using longer contact times (10 ms), we found that is possible to observe extra correlation peaks, which arise from longer range dipolar through-space interaction. These long range spectra yield further information about the structure.

^1H - ^1H multiple-Quantum Spectroscopy: Two-dimensional double-quantum (DQ) and triple-quantum (TQ) experiments were recorded on Bruker DSX-600 spectrometer with a conventional double resonance 3.2 mm CPMAS probe, according to the following general scheme³: excitation of DQ coherences, t_1 evolution, Z-filter, and detection. The spectra were recorded in a rotor synchronized fashion in t_1 ; that is the t_1 increment was set equal to one rotor period (4.545 μs). One cycle of the standard back-to-back (BABA) recoupling sequence was used for the excitation and reconversion period. Quadrature detection in w_1 was achieved using the States-TPPI method. A spinning frequency of 22 KHz was used. The 90° proton pulse length was 2.5 μs , while a recycle delay of 5 s was used. A total 128 t_1 increments with 32 scan each were recorded. Double (DQ)- and Triple (TQ)-quantum proton spectroscopies under fast MAS have recently shown to be powerful techniques to probe the structural information and dynamics inherent proton-proton dipolar couplings. The DQ frequency in the w_1 dimension corresponds to the sum of two single quantum (SQ) frequencies of the two coupled protons and correlates in the w_2 dimension with the two corresponding proton resonances. The TQ frequency in the w_1 dimension corresponds to the sum of the three SQ frequencies of the three coupled protons and correlates in the w_2 dimension with the three individual proton resonances. Conversely, groups of less than three equivalent spins will not give rise to diagonal signals in the spectrum. Two-dimensional DQ and TQ correlations experiments can thus applied to determine in a reliable way the number of attached equivalent proton.

Fourier Transformed Infrared Spectroscopy. FTIR spectra were recorded on a Nicolet 6700 FT-IR spectrometer equipped with a cell under controlled atmosphere. Typically, 16 scans were accumulated for each spectrum (resolution 4 cm^{-1}).

Nitrogen adsorption-desorption Isotherms at 77 K were measured using a Micromeritics ASAP 2024 physisorption analyzer. Specific surface areas were calculated following typical BET procedures. Pore size distribution was obtained using BJH pore analysis applied to the desorption branch of the nitrogen adsorption/desorption isotherm.

Preparation of Dichlorotrimethyl tantalum^(V) 1. The molecular precursor $\text{Ta}(\text{CH}_3)_3\text{Cl}_2$ **1** was prepared from TaCl_5 and $(\text{CH}_3)_2\text{Zn}$, following the literature procedure.⁴ The resulting powder was recrystallized in pentane at -40°C to afford pale yellow

crystals (yield 60 %). ¹H NMR (C₆D₆): 1.51 (s, 9H, Ta(CH₃)₃) ppm. ¹³C NMR (C₇D₈): 74.9 (s, Ta(CH₃)₃) ppm. Anal. Calc. for C₃H₉Cl₂Ta: C, 12.13; H, 3.05%. Found: C, 11.93; H, 2.90%.

The ¹³C enriched Ta(CH₃)₃Cl₂ was synthesized as described below.⁵ ¹³C enriched (CH₃)₂Zn was produced from a mixture of ¹³CH₃I and CH₃I (1:1). ¹³C enriched Ta(CH₃)₃Cl₂ was produced following the same procedure. (19% of ¹³C enriched material based on ¹H NMR analysis.)

Preparation of [(≡SiO)Cl₂Ta(CH₃)₂] on SBA-15, Aerosil and MCF¹. 290 mg TaMe₃Cl₂ **1** in slight excess (1.1 equivalent) with respect to the amount of surface accessible silanols (1.27 ±0.1 mmol silanol groups per gram) was reacted with 1.0 g of silica at room temperature in pentane for 2 h. After filtration and three washing cycles, all volatile compounds were condensed to quantify methane evolved during the grafting. And the solid was dried under dynamic vacuum (< 10⁻⁵ Torr, 2 h). The volatile components were analysed by GC and 0.97 ±0.1 mmol of CH₄ per gram of SBA-15₍₇₀₀₎ was determined. The reaction was monitored by FT-IR showing that 95% of isolated silanol disappeared (Fig. S3) with a concomitant appearance of intense bands at 2988-2875 cm⁻¹ and weak bands in the 1500-1300 cm⁻¹ region. Elemental analysis gave 14.8% Ta, 1.65% C and 0.39% H consistent with (≡SiO)Ta^vCl₂Me₂.

Preparation of [(≡SiO)Cl₂Ta(CH₃)₂]/Aerosil₍₇₀₀₎•NEt₃. 150 mg [(≡SiO)Cl₂Ta(CH₃)₂]/Aerosil₍₇₀₀₎ was put into a Schlenk tube equipped with a septum. After evacuation (< 10⁻⁵ Torr), 20 μl of dried NEt₃ was introduced into the tube by syringe. The white [(≡SiO)Cl₂Ta(CH₃)₂]/Aerosil₍₇₀₀₎ powder turned to light yellow immediately, the light yellow powder was evacuated (< 10⁻⁵ Torr) for 1 h to afford the product. Elemental analysis gave 5 % Ta, 0.7 % C and 0.19% H.

Table S1: Elemental analysis results of surface organometallic compounds

Element	C	H	Cl	Ta	N
[(≡SiO)Cl ₂ Ta(CH ₃) ₂]/SBA ₍₇₀₀₎	2.00	0.44	5.42	14.8	/
[(≡SiO)Cl ₂ Ta(CH ₃) ₂]/SBA ₍₁₀₀₀₎	1.14	0.25	3.26	9.01	/
[(≡SiO)Cl ₂ Ta(CH ₃) ₂]/Aerosil ₍₇₀₀₎	0.77	0.19	1.68	5.17	/
[(≡SiO)Cl ₂ Ta(CH ₃) ₂]/Aerosil ₍₁₀₀₀₎	0.35	0.15	0.88	2.73	/
[(≡SiO)Cl ₂ Ta(CH ₃) ₂]/MCF	1.37	0.31	3.89	11.02	/
[(≡SiO)Cl ₂ Ta(CH ₃) ₂]/Aerosil ₍₇₀₀₎ •NEt ₃	1.48	0.37	1.84	5.68	0.24

Preparation and Characterization of SBA-15 and SBA-15₍₇₀₀₎ The SBA-15 was prepared was synthesized according to literature.^{6,7} SBA-15 with a specific area of 884 m²/g was dehydroxylated at 700 °C for 10 h under high vacuum (< 10⁻⁵ mbar) to generate SBA-15₍₇₀₀₎. Most interestingly after thermal treatment, the overall structural features of SBA-15 and its desired properties as large specific area and narrow pore distribution are retained. After this treatment, the specific area was 802 m²/g. SBA-15 and the subsequent products were characterized by nitrogen adsorption at 77.4 K (N₂ adsorption) for determination of the specific surface, size, volume and size distribution of the pores (Table S1). The SBA-15₍₇₀₀₎ PXRD pattern clearly reveals four well-resolved peaks in the 2θ domain at 0.95, 1.60, and 1.83°. They can be respectively indexed as (100), (110), and (200) diffraction peaks associated with *p6mm* hexagonal symmetry.¹ This symmetry remains unchanged, even after dehydroxylation at 700 °C, showing the great thermal stability of such a material.

Table S2. Surface area, pore volume and effective mean pore diameter of the material SBA-15 and SBA-15 derived materials

Material	a_s	Pore Volume^a	Pore Size^b
	(m²/g)	(cm³/g)	(nm)
SBA-15	884	1.18	6.3
SBA-15 ₇₀₀	802	1.08	5.4
[(≡SiO)Cl ₂ Ta(CH ₃) ₂]/ SBA-15 ₇₀₀	649	0.77	4.7
SBA-15 ₁₀₀₀	554	0.89	5.3
Aerosil200-700	213	/	/
Aerosil200-1000	169	/	/

^aTotal pore volume at $P/P_0 = 0.967$. ^bPore size from desorption branch applying the BJH pore analysis.

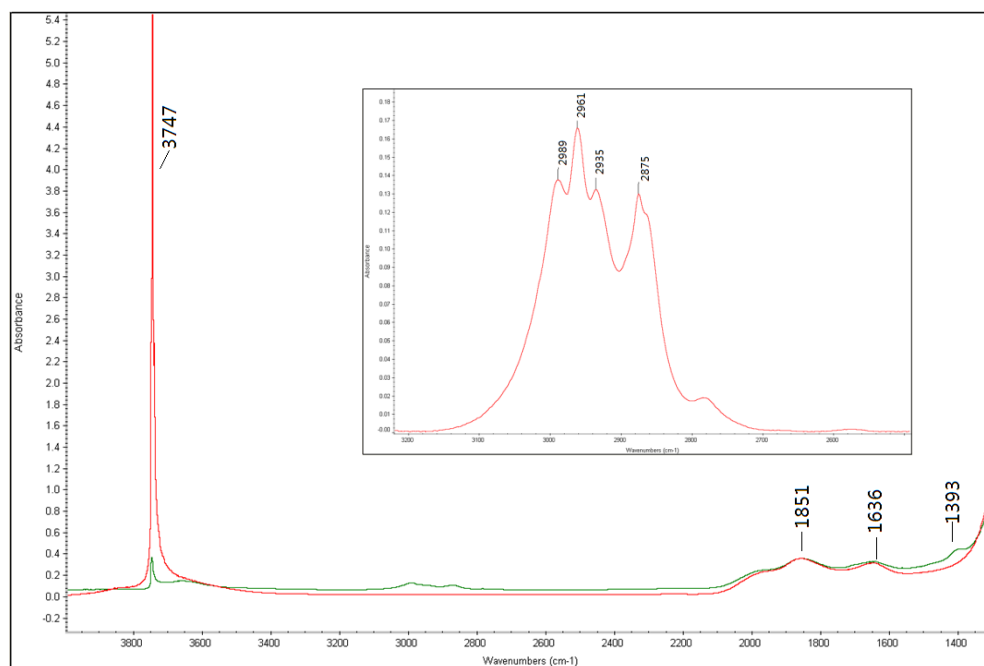


Figure S1. FT-IR spectroscopy of SBA-15 partially dehydroxylated at 700 °C (SBA-15₍₇₀₀₎) (green curve) and after grafting TaCl₂Me₃ on SBA-15₍₇₀₀₎ (red curve). Expanded IR absorbance region corresponding to alkyl groups (insert graph).

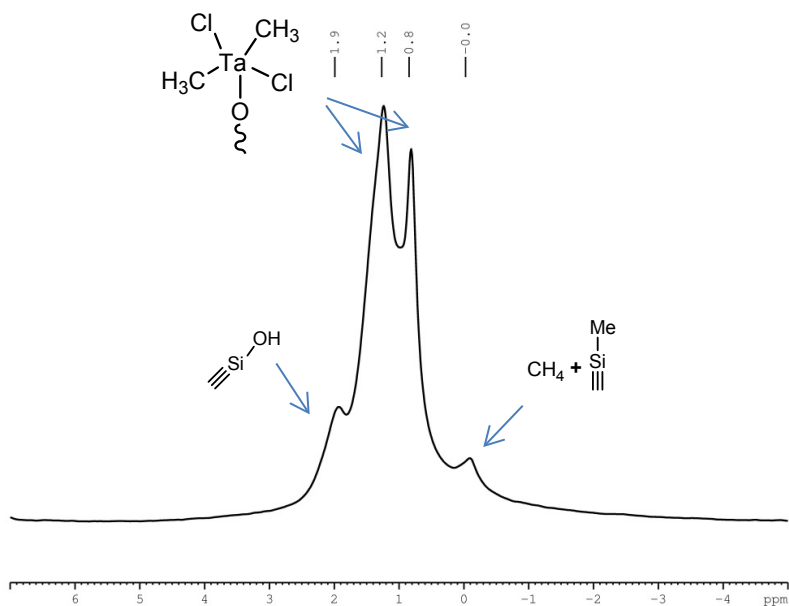


Figure S2. ¹H MAS NMR of (≡ SiO)Ta^(V)Cl₂Me₂/SBA-15₍₇₀₀₎ under MAS of 17 kHz. The number of scans was 32, and the recycle delay was set to 5 s. This compound decomposes slowly at room temperature to release methane, and Si-Me group can be produced by the reaction of Ta-Me with the surface Si-O-Si bridge, both methane and Si-Me appear in the same range in the NMR and can't be discriminated,² we assigned the peak at 0.0 ppm to be the mixture of these two.

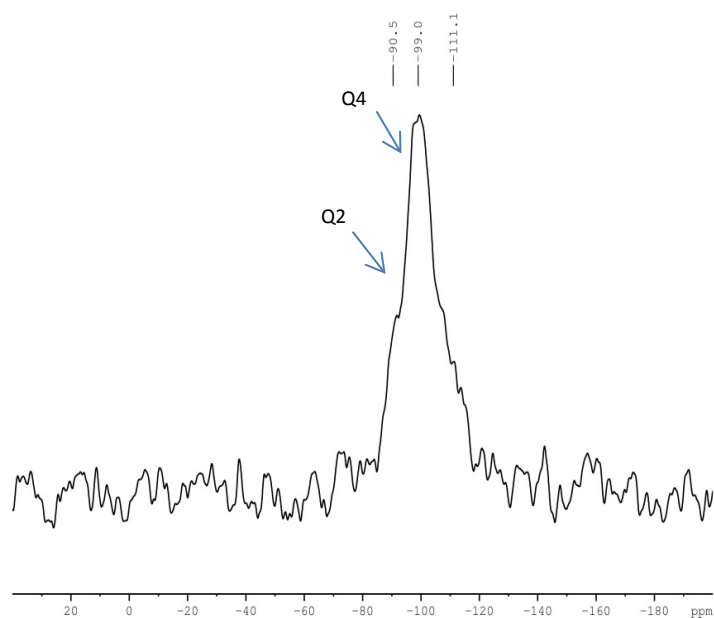


Figure S3. ^{29}Si CP/MAS NMR of $(\equiv \text{SiO})\text{Ta}^{(\text{V})}\text{Cl}_2\text{Me}_2/\text{SBA-15}_{(700)}$ under MAS of 5 kHz. The number of scans was 30000 and the recycle delay was set to 4 s. A CP step of 2 ms was used.

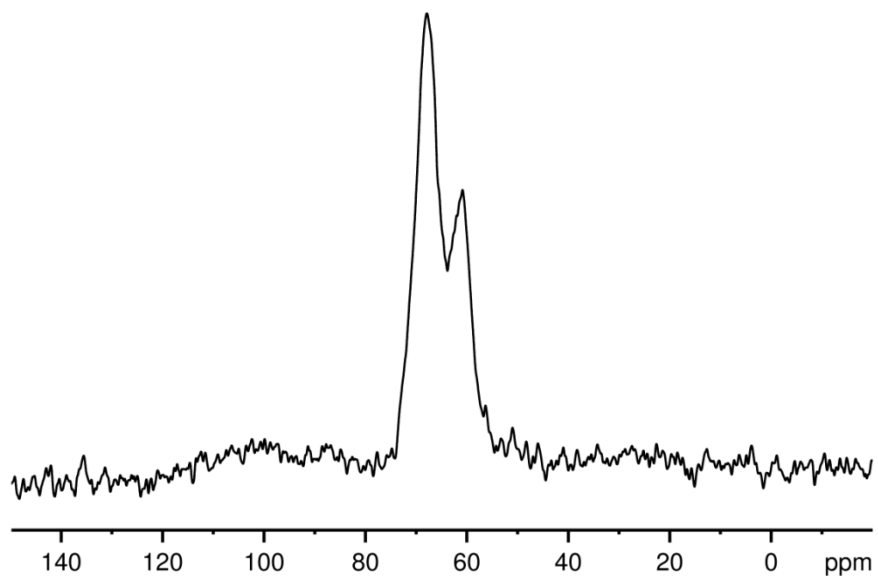


Figure S4. 1D ^{13}C CP/MAS NMR spectrum of $(\equiv \text{SiO})\text{Ta}^{(\text{V})}\text{Cl}_2\text{Me}_2/\text{SBA-15}_{(700)}$ under MAS of 10 kHz recorded using spin-echo sequence. The number of scans was 9000 and the recycle delay was set to 5 s

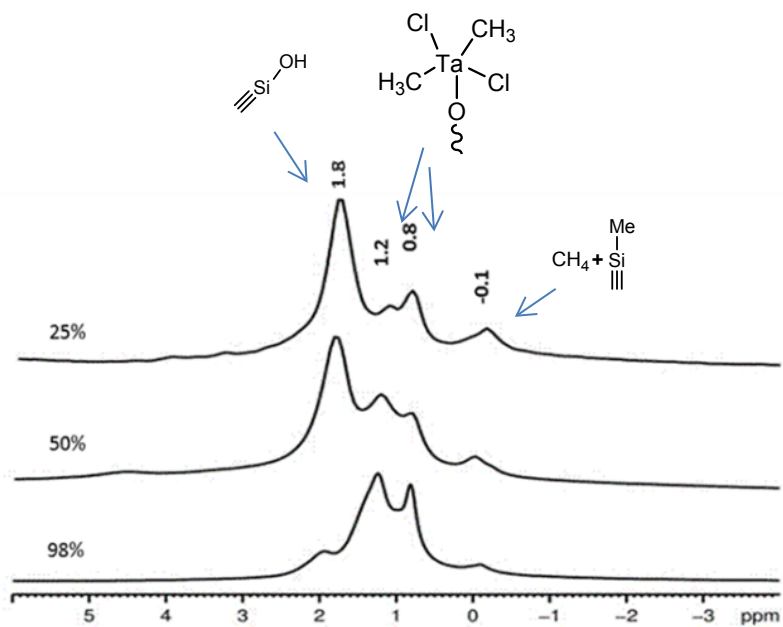


Figure S5: ^1H MAS NMR, spectra of $(\equiv\text{SiO})\text{Ta}^{(\text{V})}\text{Cl}_2\text{Me}_2/\text{SBA-15}_{(700)}$ at with 25%, 50% and 98% coverage of the surface silanols. The number of scans was 32, and the recycle delay was set to 5 s.

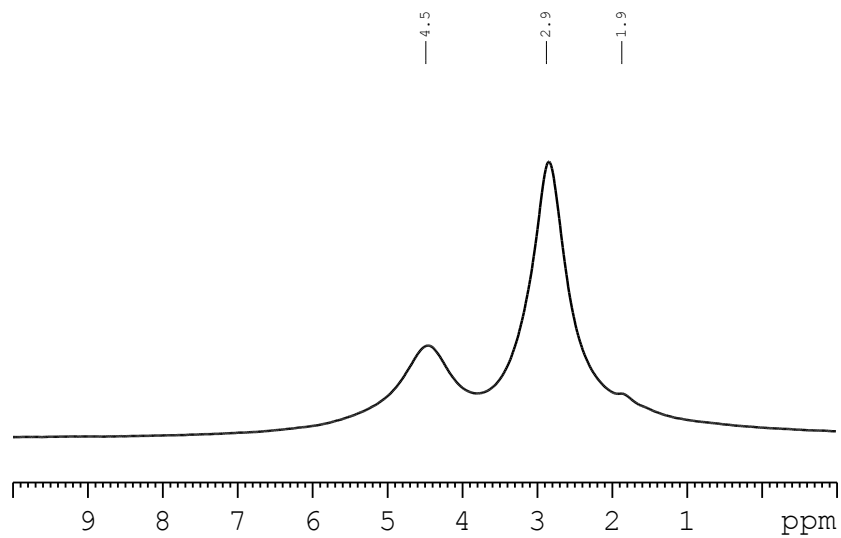


Figure S6. ^1H MAS NMR of $(\equiv\text{SiO})\text{Ta}^{(\text{V})}\text{Cl}_2\text{Me}_2/\text{Aerosil}_{(700)}\cdot\text{NET}_3$. The number of scans was 32, and the recycle delay was set to 5 s.

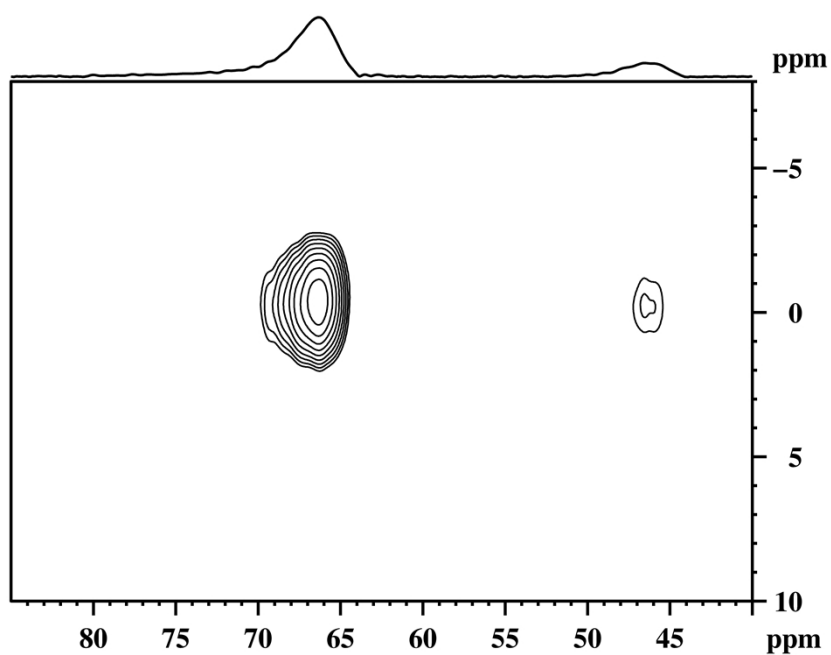


Figure S7. 2D ^1H - ^{13}C HETCOR MAS NMR spectrum of $(\equiv \text{SiO})\text{Ta}^{(\text{V})}\text{Cl}_2\text{Me}_2 / \text{Aerosil}_{(700)} \cdot \text{NEt}_3$ under MAS of 10 kHz recorded with a contact times of 5 ms.

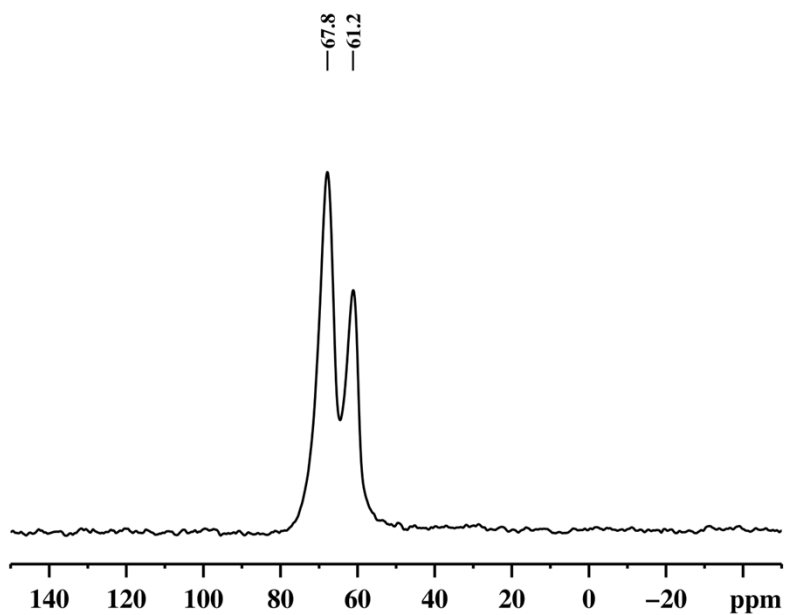


Figure S8. ^{13}C CP/MAS NMR of $(\equiv \text{SiO})\text{Ta}^{(\text{V})}\text{Cl}_2\text{Me}_2 / \text{MCF}(700)$ under MAS of 10 kHz. The number of scans was 3000, and the recycle delay was set to 5 s

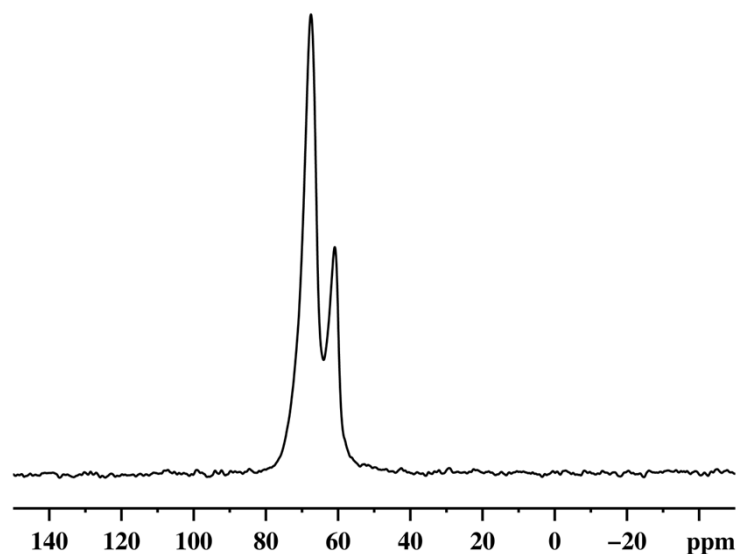


Figure S9. ^{13}C CP/MAS NMR of $(\equiv\text{SiO})\text{Ta}^{\text{V}}\text{Cl}_2\text{Me}_2/\text{Aerosil}(700)$ under MAS of 10 kHz. The number of scans was 3000, and the recycle delay was set to 5 s

Table S3: $[(\equiv\text{SiO})\text{Ta}^{\text{V}}\text{Cl}_2\text{Me}_2]$ on different support

Support	Species	Ratio
Aerosil ₍₇₀₀₎	2a (68 ppm), 2b (62 ppm)	3:1
SBA-15 ₍₇₀₀₎	2a (68 ppm), 2b (62 ppm)	2:1
MCF ₍₇₀₀₎	2a (68 ppm), 2b (62 ppm)	2:1

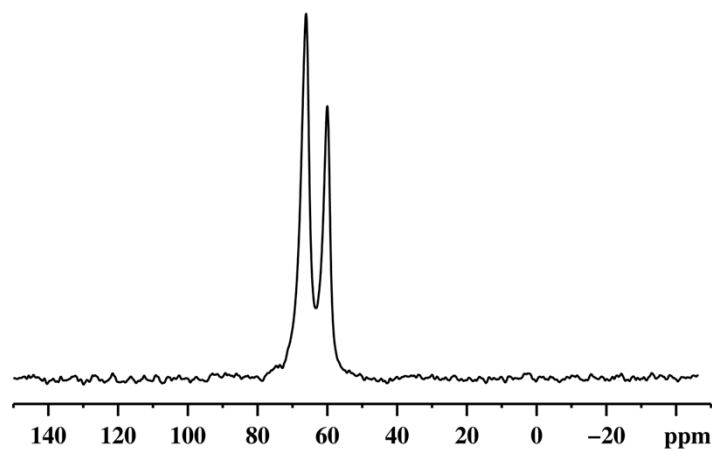


Figure S10. ^{13}C CP/MAS NMR of $(\equiv\text{SiO})\text{Ta}^{\text{V}}\text{Cl}_2\text{Me}_2/\text{SBA-15}(1000)$ under MAS of 10 kHz. The number of scans was 3000, and the recycle delay was set to 5 s

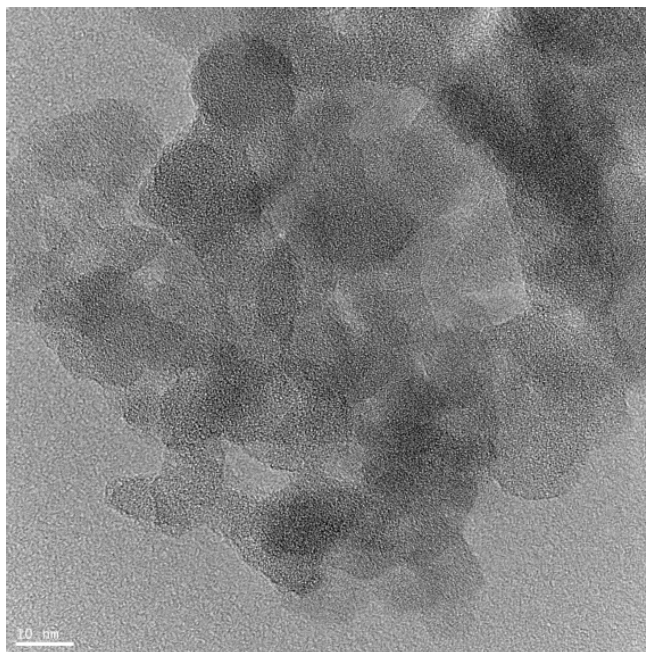


Figure S11. TEM Photo of $(\equiv \text{SiO})\text{Ta}^{(\text{V})}\text{Cl}_2\text{Me}_2/\text{Aerosil}_{(700)}$

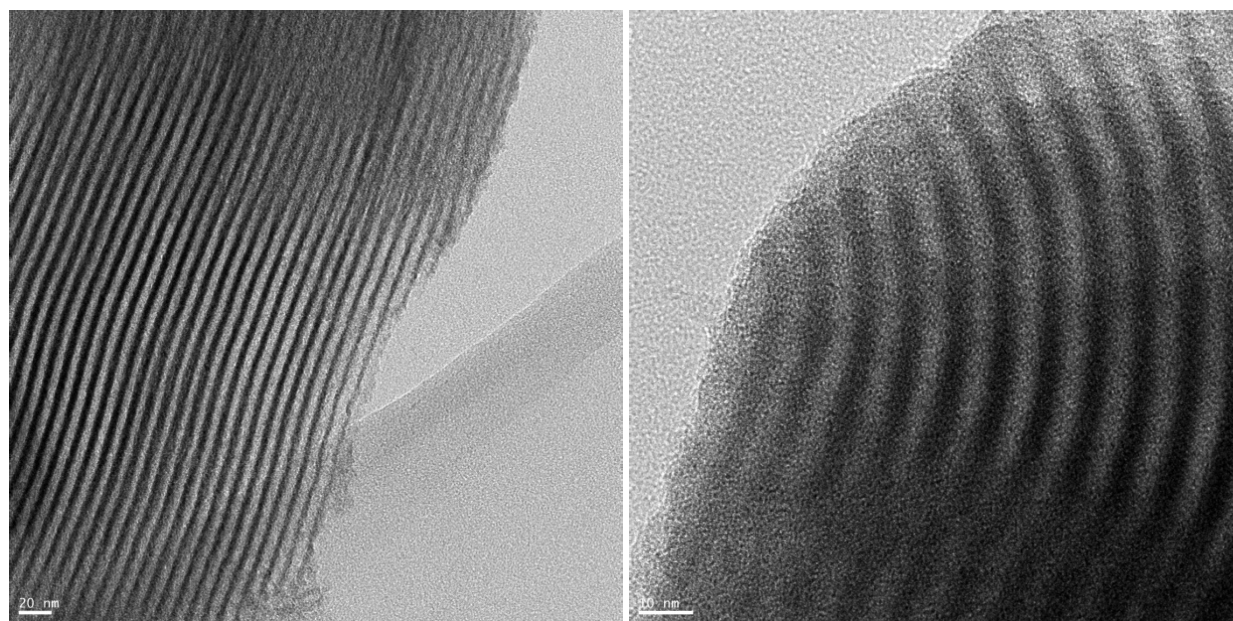
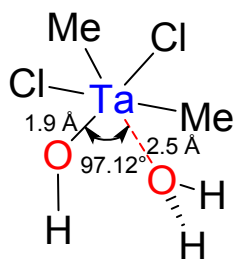


Figure S12. TEM Photo of $(\equiv \text{SiO})\text{Ta}^{(\text{V})}\text{Cl}_2\text{Me}_2/\text{SBA-15}_{(700)}$

Calculated energies, Cartesian coordinates, and NMR Chemical Shifts values ³⁻⁴

Density functional theory calculations were employed with Gaussian 09 package, utilizing the M06¹ functional of Truhlar in conjunction with basis set 6-31++G** for all nonmetal atoms in the gas phase. The small-core, quasi-relativistic Stuttgart/Dresden effective core potential, with an associated (8s7p6d)/[6s5p3d] valence basis set (SDD keywords in Gaussian09) were used for Ta. NMR Chemical Shifts values were calculated at the same level using the IGAIM and CSGT procedure. The results are summarized below.



Ta	0.09143100	-0.25629000	-0.02548000
O	-0.35391500	-1.99007400	0.56975600
O	-0.83309500	0.98870200	1.92907100
H	-0.28447300	-2.79179700	1.08954800
H	-1.62273800	1.47252700	1.64805300
H	-0.20566700	1.63756700	2.27154000
Cl	-2.15083300	0.33585200	-0.59823700
C	1.03080200	-0.97856400	-1.81623200
H	2.12311400	-0.89246200	-1.71583300
H	0.77037000	-2.02215100	-2.02454600
H	0.73670400	-0.34910600	-2.66612700
Cl	0.95454400	1.90556900	-0.60167900
C	1.61660100	-0.26845700	1.54169500
H	2.03628200	0.70437700	1.81429600
H	1.29866600	-0.80977500	2.43935000
H	2.42185100	-0.85102900	1.05897800

Calculating IGAIM nuclear magnetic shielding tensors (ppm):

1 Ta Isotropic = -185.0003 Anisotropy = 77.8185
2 O Isotropic = 70.6917 Anisotropy = 311.6132
3 O Isotropic = 259.4227 Anisotropy = 23.9265
4 H Isotropic = 26.8587 Anisotropy = 9.3239
5 H Isotropic = 28.9307 Anisotropy = 15.5438
6 H Isotropic = 29.0515 Anisotropy = 14.6793
7 Cl Isotropic = 443.8177 Anisotropy = 612.0688
8 C Isotropic = 132.7328 Anisotropy = 81.4051
9 H Isotropic = 28.5427 Anisotropy = 4.9506
10 H Isotropic = 27.6616 Anisotropy = 2.6834
11 H Isotropic = 27.7779 Anisotropy = 4.6560
12 Cl Isotropic = 356.2604 Anisotropy = 649.2099
13 C Isotropic = 138.3144 Anisotropy = 64.1390
14 H Isotropic = 28.5962 Anisotropy = 2.5442
15 H Isotropic = 28.5666 Anisotropy = 3.6873
16 H Isotropic = 29.1302 Anisotropy = 6.2573

Calculating CSGT nuclear magnetic shielding tensors (ppm):

1 Ta Isotropic = -184.9477 Anisotropy = 77.8492
2 O Isotropic = 70.6457 Anisotropy = 311.6885
3 O Isotropic = 259.3550 Anisotropy = 23.9723
4 H Isotropic = 26.8680 Anisotropy = 9.3258
5 H Isotropic = 28.9366 Anisotropy = 15.5438
6 H Isotropic = 29.0583 Anisotropy = 14.6712
7 Cl Isotropic = 443.7668 Anisotropy = 612.1123
8 C Isotropic = 132.7208 Anisotropy = 81.4199
9 H Isotropic = 28.5453 Anisotropy = 4.9380
10 H Isotropic = 27.6633 Anisotropy = 2.6843
11 H Isotropic = 27.7783 Anisotropy = 4.6432

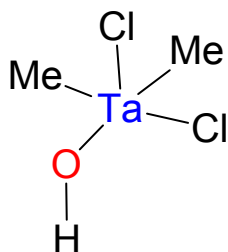
12 Cl Isotropic = 356.2315 Anisotropy = 649.2491

13 C Isotropic = 138.3079 Anisotropy = 64.1363

14 H Isotropic = 28.5997 Anisotropy = 2.5317

15 H Isotropic = 28.5716 Anisotropy = 3.6816

16 H Isotropic = 29.1365 Anisotropy = 6.2506



Ta -0.11712700 -0.16579200 0.00000700

O -1.69425400 -1.20633800 0.00020500

H -2.30671300 -1.94246000 0.00097800

C 0.48810600 -1.15077700 1.82130000

C 0.48714500 -1.15098300 -1.82134600

Cl -1.18444800 1.90200500 0.00008300

Cl 2.05796400 0.77829300 -0.00031800

H 1.17159800 -1.95969900 1.51424900

H 1.04872000 -0.48189100 2.48286800

H -0.36362000 -1.58631300 2.35278700

H 1.16650900 -1.96286600 -1.51267900

H -0.36536700 -1.58320800 -2.35427800

H 1.05185500 -0.48456100 -2.48182000

Calculating IGAIM nuclear magnetic shielding tensors (ppm):

1 Ta Isotropic = -188.4323 Anisotropy = 71.1637

2 O Isotropic = 72.4844 Anisotropy = 269.8554

3 H Isotropic = 27.2101 Anisotropy = 8.5952

4 C Isotropic = 137.1066 Anisotropy = 67.5667
5 C Isotropic = 137.0214 Anisotropy = 67.6558
6 Cl Isotropic = 322.9463 Anisotropy = 758.4720
7 Cl Isotropic = 258.8691 Anisotropy = 727.5940
8 H Isotropic = 28.7050 Anisotropy = 6.3680
9 H Isotropic = 27.9158 Anisotropy = 4.4348
10 H Isotropic = 28.1115 Anisotropy = 3.5400
11 H Isotropic = 28.7115 Anisotropy = 6.3899
12 H Isotropic = 28.1069 Anisotropy = 3.5469
13 H Isotropic = 27.9089 Anisotropy = 4.4272

Calculating CSGT nuclear magnetic shielding tensors (ppm):

1 Ta Isotropic = -188.4022 Anisotropy = 71.2208
2 O Isotropic = 72.4444 Anisotropy = 269.9334
3 H Isotropic = 27.2225 Anisotropy = 8.5946
4 C Isotropic = 137.1036 Anisotropy = 67.5668
5 C Isotropic = 137.0184 Anisotropy = 67.6558
6 Cl Isotropic = 322.8812 Anisotropy = 758.5620
7 Cl Isotropic = 258.8305 Anisotropy = 727.6333
8 H Isotropic = 28.7132 Anisotropy = 6.3593
9 H Isotropic = 27.9219 Anisotropy = 4.4209
10 H Isotropic = 28.1191 Anisotropy = 3.5422
11 H Isotropic = 28.7197 Anisotropy = 6.3814
12 H Isotropic = 28.1145 Anisotropy = 3.5490
13 H Isotropic = 27.9149 Anisotropy = 4.4132

The O-Ta-O angle effect on the chemical shift values was checked. We calculated the chemical shift values under different O-Ta-O angle (87° - 107° in below figure). It can be found that the chemical shift difference between the two cases is $\sim 5.16 \pm 3.00$ ppm.

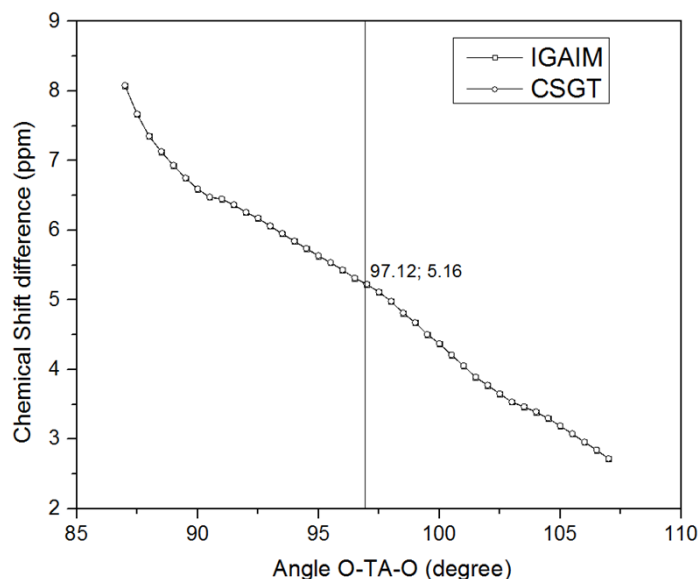


Figure S13: The plot of chemical shift difference with (O-Ta-O 87°-107°) in angle obtained by DFT calculation.

References

1. P. Schmidt-Winkel, W. W. Lukens, Jr., D.Y. Zhao, Peidong Yang, B. F. Chmelka and G. D. Stucky, *J. Am. Chem. Soc.* 1999, **121**, 254.
2. (a) Y. Chen, E. Callens, E. Abou-Hamad, N. Merle, A. J. P. White, M. Taoufik, C. Copéret, E. Le Roux and J.-M. Basset, *Angew. Chem. Int. Ed.* 2012, **51**, 11886. (b) Y. Chen, E. Callens, E. Abou-hamad and J.-M. Basset, *J. Organomet. Chem.*, 2013, **744**, 3. (c) Millot, N.; Soignier, S.; Santini, C. C.; Baudouin, A.; Basset, J.-M. *J. Am. Chem. Soc.* 2006, **128**, 9361. (d) Jezequel, M.; Dufaud, V.; Ruiz-Garcia, M. J.; Carrillo-Hermosilla, F.; Neugebauer, U.; Niccolai, G. P.; Lefebvre, F.; Bayard, F.; Corker, J.; Fiddy, S.; Evans, J.; Broyer, J.-P.; Malinge, J.; Basset, J.-M. *J. Am. Chem. Soc.* 2001, **123**, 3520.
3. Gaussian 09; Revision A.2: M. J. Frisch, G. W. Trucks, H. B. Schlegel, G. E. Scuseria, M. A. Robb, J. R. Cheeseman, G. Scalmani, V. Barone, B. Mennucci, G. A. Petersson, H. Nakatsuji, M. Caricato, X. Li, H. P. Hratchian, A. F. Izmaylov, J. Bloino, G. Zheng, J. L. Sonnenberg, M. Hada, M. Ehara, K. Toyota, R. Fukuda, J. Hasegawa, M. Ishida, T. Nakajima, Y. Honda, O. Kitao, H. Nakai, T. Vreven, Jr., J. A. Montgomery, J. E. Peralta, F. Ogliaro, M. Bearpark, J. J. Heyd, E. Brothers, K. N. Kudin, V. N. Staroverov, R. Kobayashi, J. Normand, K. Raghavachari, A. Rendell, J. C. Burant, S. S. Iyengar, J. Tomasi, M. Cossi, N. Rega, N. J. Millam, M. Klene, J. E. Knox, J. B. Cross, V. Bakken, C. Adamo, J. Jaramillo, R. Gomperts, R. E. Stratmann, O. Yazyev, A. J. Austin, R. Cammi, C. Pomelli, J. W. Ochterski, R. L. Martin, K. Morokuma, V. G. Zakrzewski, G. A. Voth, P. Salvador, J. J. Dannenberg, S. Dapprich, A. D. Daniels, Ö. Farkas, J. B. Foresman, J. V. Ortiz, J. Cioslowski, D. Fox, J. Gaussian, Inc.: Wallingford, CT, 2009.
4. (a) R. W. Ditchfie, J. Hehre, J. A. Pople, *J. Chem. Phys.* 1971, **54**, 724. (b) W. J. Hehre, R. Ditchfie, J. A. Pople, *J. Chem. Phys.* 1972, **56**, 2257. (c) P. C. Harihara, J. A. Pople, *Theor. Chim. Acta* 1973, **28**, 213. (d) M. Dolg, U. Wedig, H. Stoll, H. Preuss, *J. Chem. Phys.* 1987, **86**, 866. (e) D. Andrae, U. Haussermann, M. Dolg, H. Stoll, H. Preuss, *Theor. Chim. Acta* 1990, **77**, 123.